Environmental Science Processes & Impacts

Evidence for non-electrostatic interactions between a pyrophosphate-functionalized uranyl peroxide nanocluster and iron (hydr)oxide minerals

Journal:	*Environmental Science: Processes & Impacts*
Manuscript ID	EM-ART-03-2019-000139.R1
Article Type:	Paper
Date Submitted by the Author:	03-Jun-2019
Complete List of Authors:	Sadergaski, Luke; University of Notre Dame, Civil & Environmental Engineering & Earth Sciences Perry, Samuel; University of Notre Dame, Civil & Environmental Engineering & Earth Sciences Tholen, Luke; University of Notre Dame, Civil & Environmental Engineering & Earth Sciences Hixon, Amy; University of Notre Dame, Civil & Environmental Engineering & Earth Sciences

ARTICLE

Evidence for non-electrostatic interactions between a pyrophosphate-functionalized uranyl peroxide nanocluster and iron (hydr)oxide minerals

Received 00th January 20xx,
Accepted 00th January 20xx

DOI: 10.1039/x0xx00000x

Luke R. Sadergaski,[a] Samuel N. Perry,[a] Luke R. Tholen,[a] and Amy E. Hixon *[a]

The terminal oxygen atoms of the pyrophosphate groups in the uranyl peroxide nanocluster $U_{24}Pp_{12}$ ($[(UO_2)_{24}(O_2)_{24}(P_2O_7)_{12}]^{48-}$) are not fully satisfied by bond valence considerations and can become protonated. This functionality could allow for specific interactions with mineral surfaces, as opposed to the electrostatically-driven interactions observed between non-functionalized uranyl peroxide nanoclusters and mineral surfaces. The sorption of $U_{24}Pp_{12}$ to goethite and hematite was studied using batch sorption experiments as a function of $U_{24}Pp_{12}$ concentration, mineral concentration, and pH. A suite of spectroscopic techniques, scanning electron microscopy, and electrophoretic mobility measurements were used to examine the minerals before and after reaction with $U_{24}Pp_{12}$, leading to a proposed conceptual model for $U_{24}Pp_{12}$ interactions with goethite. The governing rate laws were determined and compared to those previously determined for a non-functionalized uranyl peroxide nanocluster. The rate of uranyl peroxide nanocluster sorption depends on the charge density and functionalized component of the uranyl peroxide cage. Electrophoretic mobility and attenuated total reflectance Fourier transform infrared spectroscopy analyses show that an inner-sphere complex forms between the $U_{24}Pp_{12}$ cluster and the goethite surface through the terminal pyrophosphate groups, leading to a proposed conceptual model in which $U_{24}Pp_{12}$ interacts with the triply-coordinated reactive sites on the (110) plane of goethite. These results demonstrate that the behavior of $U_{24}Pp_{12}$ at the iron (hydr)oxide-water interface is unique relative to interactions of the uranyl ion and non-functionalized uranyl peroxide nanoclusters.

Environmental Significance

Nuclear energy could be a key component of clean energy generation, but the safe disposal of used nuclear fuel is one barrier to expansion of the industry. Geologic repositories are the accepted solution for nuclear waste disposal; licensing them requires long-term predictions of uranium fate and transport. The recent discovery of uranyl peroxide nanoclusters leads to the concern of a uranium source term that is not included in current predictive models. In this study, we used a functionalized nanocluster and report the first evidence of an irreversible, non-electrostatic interaction at the mineral surface. These findings suggest that some uranyl peroxide nanoclusters are immobilized under environmentally-relevant conditions and highlights the importance of studying the behavior of nanomaterials at the mineral-water interface.

[a] *Department of Civil & Environmental Engineering & Earth Sciences, University of Notre Dame, Notre Dame, IN 46556 USA.*

Electronic Supplementary Information (ESI) available: ESI-MS, XPS, and SEM-EDS methodologies; extended description of the approach used to determine the governing rate laws; pXRD and Raman spectra of goethite and hematite; figures showing the % U removed as a function of goethite concentration, hematite concentration, and $U_{24}Pp_{12}$ concentration; SEM micrographs, XPS spectra, and Raman spectra; tables of experimental conditions and raw data. See DOI: 10.1039/x0xx00000x

Introduction

High concentrations of CO_2 and other greenhouse gases in the atmosphere are projected to increase global temperatures and affect the planet's ability to sustain the life of billions of people. As global energy demand continues to increase, the need to phase out fossil fuels and replace them with clean energy sources is becoming more critical. Nuclear energy could be an attractive form of clean energy, as no greenhouse gases are emitted during power production, but the lack of a permanent storage or disposal solution for used nuclear fuel remains at the forefront of public concern.

Deep geologic repositories are generally accepted as the best approach for disposing of intermediate- and high-level nuclear waste.[1,2] Although many countries are in various stages of siting, licensing, and constructing a permanent disposal facility, there is no fully-operational facility for used nuclear fuel. Nuclear repositories will be specially designed to maintain their integrity for millions of years by using both natural and engineered barriers. These containment systems will eventually fail and release radionuclides into the environment. The actinide elements, such as uranium, are of particular concern due

to their radiotoxicity and long half-lives. Some repository designs include the addition of cementitious materials or MgO barriers, which ultimately moderate the pH of any leachate to the hyperalkaline region.[2] U(VI) is generally expected to have a low solubility under these conditions.

Within the last decade, a large family of uranyl peroxide nanoclusters has been synthesized and characterized.[3] In general, the exterior and interior of these nanoclusters are truncated by the oxygen atoms of uranyl ions (i.e., -yl oxygens) and adjacent uranyl ions are connected through bridging peroxide groups or other ligands (e.g., hydroxyl, phosphate, pyrophosphate, nitrate, oxalate, and phosphite).[4] Although these nanoclusters have not been directly observed in nature, it is possible that uranyl peroxide species could form under conditions where the radiation-driven radiolysis of water produces hydrogen peroxide.[5] Thus, uranyl peroxide species and nanoclusters could form at uranium ore deposits, in the vicinity of used nuclear fuel, and at contaminated locations such as the Hanford Site, Fukushima-Daiichi, and the Savannah River Site.[6–8] Because these nanoclusters have properties of both dissolved species and colloids, studying their behavior at the mineral-water interface is critically important and necessary in order to predict their behavior in natural systems.

Goethite (α-FeOOH) and hematite (α-Fe_2O_3) are the most common iron (hydr)oxide minerals in the environment and are important sorbents for uranium.[8–11] Although the adsorption behavior of the uranyl ion is fairly well established, clear differences between uranyl peroxide nanoclusters and the discrete uranyl ion suggest that the mechanisms governing their interactions with charged surfaces will be different and could give rise to significant environmental implications.[12–14] Therefore, examining the mineral-water interface chemistry of uranyl nanoclusters is warranted in order to more comprehensively assess the effectiveness of radionuclide remediation strategies and predict the long-term validity of nuclear waste disposal in geologic repositories.

Two studies have considered the sorption of a non-functionalized uranium polyoxometalate nanocluster $[(UO_2)(O_2)(OH)]_{60}^{60-}$ (U_{60}) to the natural minerals goethite and hematite.[12,13] These studies found that U_{60} sorbs via weak, outer-sphere, electrostatic interactions between the negatively-charged nanocluster and the positively-charged mineral surface. The oxygen atoms of the uranyl ion are relatively inert and can only act as H-bonding acceptors or bind to highly coordinated alkali cations.[15] Comparatively, the uranyl peroxide nanocluster $[(UO_2)_{24}(O_2)_{24}(P_2O_7)_{12}]^{48-}$ ($U_{24}Pp_{12}$) has a thinner electric double layer (EDL), which is consistent with a higher charge-to-surface area ratio than U_{60}, and is pyrophosphate functionalized.[16,17] When crystallized, the negatively-charged cage is balanced by Li^+ and Na^+ cations, both inside the cage and in the interstitial space between cages, with the chemical formula $Li_{48-x}Na_x[(UO_2)_{24}(O_2)_{24}(P_2O_7)_{12}]\cdot nH_2O$, (x≈24 and n≈120).[18] In solution, the cage persists as an aqueous species and retains an effective negative charge.[16,19] Both U_{60} and $U_{24}Pp_{12}$ have notably high solubility ((1.77 ± 0.11) x 10^5 ppm U and (2.94 ±0.17) x 10^5 ppm U, respectively) in the high-pH regime.[16]

The terminal oxygen atoms of the pyrophosphate groups in $U_{24}Pp_{12}$ are not fully satisfied by bond valence considerations and can become protonated.[20,21] This functionality could allow for the formation of specific, inner-sphere sorption complexes. When comparing $U_{24}Pp_{12}$ to U_{60}, we are mainly interested in understanding how the terminal oxygen atoms of the uranyl peroxide cage, either –yl oxygen atoms of the uranyl ion or the oxygen atoms of the pyrophosphate unit (highlighted in Figure 1), may or may not dictate sorption interactions with functional groups on mineral surfaces.

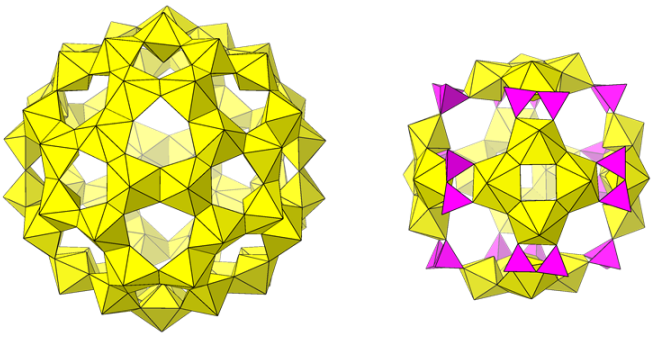

Figure 1. Polyhedral representations of U_{60} (left) and $U_{24}Pp_{12}$ (right). The $[(UO_2)(O_2)_2(OH)_2]$ and $[(UO_2)(O_2)_2]$ subunits of U_{60} and $U_{24}Pp_{12}$, respectively, are represented by yellow hexagonal bipyramid polyhedrons. Pyrophosphate linkages are represented as phosphate polyhedra shown in magenta. Alkali counter-cations have been removed for clarity. The U_{60} nanocluster is approximately 2.5 nm in diameter whereas the $U_{24}Pp_{12}$ cluster is approximately 1.8 nm in diameter.

This study examines the sorption kinetics of $U_{24}Pp_{12}$ to goethite and hematite as a function of time, $U_{24}Pp_{12}$ concentration (0.5 – 2 g L^{-1}), mineral concentration (100 – 500 m^2 L^{-1}), and pH (8 – 9). It also characterizes the reacted mineral phase using a variety of analytical techniques. The purpose of this work is two-fold: (1) to determine the governing rate law describing sorption of $U_{24}Pp_{12}$ to goethite and hematite, and (2) to describe how pyrophosphate functionality affects uranyl peroxide nanocluster sorption reactions. Comparing the sorption of $U_{24}Pp_{12}$ and U_{60} to goethite and hematite will aid in the elucidation of molecular-scale mechanisms governing uranyl peroxide nanocluster interactions at the mineral-water interface.

Methods

Caution: Depleted uranium was used in these experiments. It is radioactive and should only be handled by trained

workers in approved facilities! All chemicals were commercially obtained (ACS grade) and used as received unless otherwise stated. Additional methodologies describing electrospray ionization mass spectrometry (ESI-MS), X-ray photoelectron spectroscopy (XPS) and scanning electron microscopy (SEM) analyses are provided in the Supporting Information.

$U_{24}Pp_{12}$ preparation and characterization

Crystals containing $U_{24}Pp_{12}$ nanoclusters were synthesized according to published procedures.[18] Crystals were collected with a Buchner funnel, rinsed with Milli-Q water (18.2 MΩ cm at 25°C), and dissolved in Milli-Q water to make a 60 g L^{-1} stock solution of $U_{24}Pp_{12}$. Single crystal X-ray diffraction (SC-XRD) was used to identify several $U_{24}Pp_{12}$ crystals within the triclinic crystal system (space group $P\overline{1}$) and unit cell parameters were in good agreement with published data. SC-XRD data were collected at 100 K using a Bruker APEXII Quazar single-crystal diffractometer with graphite-monochromated Mo Kα X-ray radiation. The $U_{24}Pp_{12}$ stock solution was characterized using electrospray ionization mass spectrometry (ESI-MS).[22]

Goethite and hematite synthesis and characterization

Goethite and hematite were synthesized according to the methods of Schwertmann and Cornell[23] and characterized by powder X-ray diffraction (10-70° 2-theta, Cu-Kα radiation), Raman spectroscopy, and BET. Powder patterns and Raman spectra are provided in Figures S1-S3. The specific surface areas of goethite and hematite used in this study were 30.2 m^2 g^{-1} and 31.5 m^2 g^{-1}, respectively.

Phase analysis light scattering

Phase analysis light scattering was used to determine the isoelectric point by measuring the zeta potential of goethite and hematite powder samples (0.25 g L^{-1}), using a Brookhaven NanoBrook Omni instrument, as a function of pH. Triplicate zeta potential measurements were modeled using Smoluchowsky calculations to determine an isoelectric point (IEP) of 9.13 ± 0.07 and 8.86 ± 0.06 for goethite and hematite, respectively, at the 95% confidence interval, which is in good agreement with published results.[24,25] The IEP of each mineral phase was also measured after reactions with $U_{24}Pp_{12}$. Suspensions containing 1 g L^{-1} $U_{24}Pp_{12}$ and 500 m^2 L^{-1} goethite or hematite were equilibrated for 24 hours. Each mineral phase was collected by centrifugation, the resulting sample was re-suspended in solution (0.25 g L^{-1}), and the pH was adjusted prior to IEP measurements.

ICP-OES analysis

Inductively coupled plasma optical emission spectroscopy (ICP-OES) was used to measure the elemental concentrations in reactor solutions. Elemental concentrations were acquired using a PerkinElmer Optima 8000 DV ICP-OES instrument with 165 – 800 nm coverage and a resolution of approximately 0.01 nm for multi-elemental analysis. External calibration was used to determine the unknown elemental concentrations of U (0.2 to 20 ppm), P (0.1 to 5 ppm), Na (0.1 to 5 ppm), Li (0.025 to 1 ppm), and Fe (0.05 to 5 ppm). Aliquots from each reactor were dissolved in 10 mL of 5% nitric acid. An internal standard (1 ppm Y) was added to each standard, blank, and sample to monitor for instrument drift. Dilutions were measured gravimetrically, using an OHAUS model AX124/E balance with an accuracy of ±0.0001 g.

Raman and FT-IR spectroscopy

Attenuated total reflectance Fourier transform infrared (ATR-FTIR) spectra were recorded using a Bruker Tensor 27 FTIR spectrometer equipped with an IR source (U-shaped silicon carbide piece), a detector (W168-5/B) for middle-IR measurements, and a platinum ATR single reflection sampling accessory (A225/QI). For each sample, 128 scans in the 4000-400 cm^{-1} (MIR) spectral range were recorded with a resolution of 4 cm^{-1}. Approximately 1 mg of sample was pressed with a micrometer-controlled compression clamp to assure good contact between the sample and diamond crystal. Background correction was applied using Bruker software. Deconvolution of ATR-FTIR data was accomplished using OriginPro Data analysis and Graphing Software. During our analysis, frequencies lower than 960 cm^{-1} were not considered due to overlap with the IR-active bands of goethite and hematite resulting from complicated stretching–bending coupling modes.

Raman spectra were collected using a video-assisted Renishaw invia Raman system equipped with a 785 nm laser source and a 5x microscope objective. Spectra were collected using 1% laser power and several, 10-second scans over the range 100-3200 cm^{-1} with 2 cm^{-1} resolution.

Batch sorption and desorption experiments

Batch sorption experiments were performed in duplicate by spiking the appropriate amount of the $U_{24}Pp_{12}$ stock solution into suspensions containing 100 m^2 L^{-1} – 500 m^2 L^{-1} mineral (see Tables S1 and S2 for exact experimental conditions). The $U_{24}Pp_{12}$ concentrations (0.5 – 2 mg mL^{-1} $U_{24}Pp_{12}$; 230 – 920 ppm U) used here are consistent with or lower than other studies probing the properties of uranyl peroxide nanoclusters and are necessary to meet instrument detection limits. The concentration of U in ppm, determined by ICP-OES, was converted to grams of $U_{24}Pp_{12}$ per liter by assuming 0.468 g of U per g of $U_{24}Pp_{12}$ based on its chemical formula in the crystalline state.[18] Reactors were sampled at various time points within a week time frame. At each time point, a 300 µL aliquot was centrifuged for 8 min at 9,200 rpm and then diluted for ICP-OES analysis. In general, the pH of the reactors was constant at pH 9.0 without adjustment. If adjustment was

needed, dilute hydrochloric (HCl) was added. A glass pH probe, manufactured by Thermo Fisher Scientific (ORION 9103SC) was used to measure pH. The probe was placed in 0.001 M HCl for approximately ten minutes before each measurement in order to remove any soluble salts that might affect the stability of the nanoclusters. Controls containing only $U_{24}Pp_{12}$ in Milli-Q water were also analyzed in the same fashion to monitor $U_{24}Pp_{12}$ stability.

Desorption experiments were performed in duplicate with 1 mg mL^{-1} $U_{24}Pp_{12}$ and either 500 m^2 L^{-1} goethite or hematite. Reactors were allowed to equilibrate for two days and the solid was collected by centrifugation, rinsed with Milli-Q water, and re-suspended for one week in Milli-Q water that was either not pH-adjusted or adjusted to pH 9 or 10 using lithium hydroxide (LiOH). Aliquots of the resulting supernatant were obtained in the same manner as those from sorption experiments and run on ICP-OES and ESI-MS.

Kinetic analysis

A full description of the kinetic analysis can be found elsewhere[12] and additional details are provided in the Supporting Information. Equation 1 represents the governing rate law describing the interaction of $U_{24}Pp_{12}$ nanoclusters with goethite and hematite.

$$\frac{d[U_{24}Pp_{12}]}{dt} = -k_{rxn}[U_{24}Pp_{12}]^a[\text{mineral}]^b \quad (1)$$

In order to determine the reaction order with respect to $U_{24}Pp_{12}$ concentration, *a*, the reaction order with respect to mineral concentration, *b*, and the reaction rate constant, k_{rxn}, batch sorption experiments were set up as described above with three different mineral and three different $U_{24}Pp_{12}$ concentrations.

Results and Discussion

$U_{24}Pp_{12}$ sorption as a function of time, $U_{24}Pp_{12}$, and mineral concentration

Nanocluster and mineral concentrations were varied in batch sorption experiments in order to determine the rate law describing $U_{24}Pp_{12}$ sorption in systems containing goethite and hematite at pH 9. The percentage of uranium removed from solution increased with increasing mineral concentration in systems containing goethite and hematite (see Figures S4 and S5, respectively). As the goethite and hematite concentrations increased from 100 m^2 L^{-1} to 500 m^2 L^{-1}, more surface binding sites became available and a larger fraction of $U_{24}Pp_{12}$ was removed. Each system appeared to reach steady-state within the time frame of this study (i.e., within 24 hours).

The fraction of uranium removed from solution decreased with increasing $U_{24}Pp_{12}$ concentration (see Figures S6-S7). As the $U_{24}Pp_{12}$ concentration increased (0.5 to 2 g L^{-1}) at constant mineral concentration, the mineral binding sites became saturated and a smaller fraction (though greater mass) of $U_{24}Pp_{12}$ was removed from solution. This trend is expected to continue until the mineral capacity is reached. In each case, complete removal of the nanoclusters from solution was not attained. As a result, sorption in these systems appeared to be site-limited.

However, a site density calculation shows that this is not the case. Assuming the conservative approximation that our goethite sample has 2.3 sites nm^{-2},[26,27] there are 1.85 mmol sites per L in reactors containing 500 m^2 L^{-1} goethite. The system containing 2 mg mL^{-1} $U_{24}Pp_{12}$—which exhibited a larger loading than the 0.5 and 1 mg mL^{-1} $U_{24}Pp_{12}$ systems at pH 9—contains 0.17 mmol·L^{-1} $U_{24}Pp_{12}$. Since the concentration of mineral binding sites is an order of magnitude higher than the total concentration of $U_{24}Pp_{12}$, all of the mineral binding sites were not fully occupied. In this system (i.e., 2 mg mL^{-1} $U_{24}Pp_{12}$, 500 m^2 L^{-1} goethite), 40% of the $U_{24}Pp_{12}$ was removed, which means that there are 0.068 mmol $U_{24}Pp_{12}$ (i.e., 4.0 x 10^{19} nanoclusters) associated with 5 x 10^{20} nm^2 of goethite. Dividing the surface area by the number of $U_{24}Pp_{12}$ nanoclusters yields 12.5 nm^2 per nanocluster and suggests that each nanocluster is separated by a center-to-center distance of 3.5 nm and occupies 29 binding sites. Less sorption was observed in the hematite system and similar calculations suggest a center-to-center distance of 4.1 nm.

Based on the crystallographic radius of $U_{24}Pp_{12}$ (1.13 nm), we would expect that the center-to-center distance of nanoclusters associated with the goethite surface would be greater than 2.26 nm. If nanoclusters pack closer than 2.26 nm, it would imply aggregation or 'stacking' of the clusters on the surface. It was previously determined theoretically and experimentally that Na/Li $U_{24}Pp_{12}$ nanoclusters in the aqueous phase approach a center-to-center distance of 3.2 – 3.6 nm near the solubility limit ($2.94 \pm 0.17 \times 10^5$ ppm U or 1.82 mol of U per kg of H_2O) and are separated by ~1.3 nm from the terminal oxygen atoms truncating the nanocages.[16] The center-to-center packing distances calculated in this study are nearly identical to those found in saturated solutions. The electric double layer surrounding discrete nanoclusters restricts closer packing in saturated solutions and these sorption studies suggest that the packing of $U_{24}Pp_{12}$ on the surface of goethite may be restricted in part by the electric double layers surrounding each nanocluster. This indicates that the initial sorption interactions of $U_{24}Pp_{12}$ may be driven by outer-sphere, electrostatic interactions.

$U_{24}Pp_{12}$ is packed more densely than U_{60} (3.5 nm vs. 6.5 nm) under the same experimental conditions.[12] U_{60} is expected to pack as close as 5 to 5.7 nm at its solubility

limit,[16] which was not observed until pH 8.[12] This suggests that $U_{24}Pp_{12}$ is more reactive than U_{60}, which may be attributed to the greater charge density,[17] thinner electric double layer,[16] and stronger surface complexes formed by interactions with the pyrophosphate groups of the uranyl peroxide cage.

Inductively coupled plasma optical emission spectroscopy (ICP-OES) was also used to measure the concentrations of phosphorous, sodium, and lithium in the aqueous phase as a function of time. Na^+ and Li^+ cations are present from the dissolution of $U_{24}Pp_{12}$ crystals during preparation of the stock solution. P was removed in a similar fashion compared to U, which indicates that the $U_{24}Pp_{12}$ nanoclusters are removed from solution intact. The concentration of Na^+ decreased at a rate similar to that of uranium and was removed from solution to a greater extent than Li^+ (see Figure S8), which is in agreement with previous findings that suggest Na^+ is more strongly associated with the cage than Li^+.[16] However, in each case a smaller fraction of Na^+ and Li^+ were removed relative to U, indicating that the $U_{24}Pp_{12}$ nanocluster sorbs as an anion. These results also agree with the results of previous sorption studies in systems containing of U_{60} and goethite/hematite, which demonstrated that K^+ leaves solution with the uranyl peroxide cage while Li^+ does not.[12,13]

Governing rate laws for $U_{24}Pp_{12}$ interactions with goethite and hematite

Sorption curves presented in the Supporting Information were used to determine the reaction rate constant (k_{rxn}) and reaction orders with respect to $U_{24}Pp_{12}$ concentration (a) and mineral concentration (b). The reaction orders with respect to goethite and hematite, obtained from log-log plots of k'_{rxn} versus mineral concentration (see Figures S30 and S26, respectively), were determined to be 0.61 ± 0.03 and 1.05 ± 0.04, respectively. This indicates that the kinetics with respect to hematite are approximately first order, but that a more intricate relationship exists for the goethite system. Similarly, linear regressions were used to obtain the reaction orders as a function of $U_{24}Pp_{12}$ concentration from log-log plots of k'_{rxn} versus the nanocluster concentration (see Figures S31 and S27). The reaction order terms, a, were 0.51 ± 0.02 and 0.12 ± 0.01 for the goethite and hematite systems, respectively. This indicates that the $U_{24}Pp_{12}$ concentration has a weaker influence on the reaction rate in the hematite system than in the goethite system. The reaction order terms a and b in the goethite system are very similar whereas the reaction terms in the hematite system are different by nearly an order of magnitude. The reaction order term a is also much greater in the goethite system than the hematite system and therefore the sorption of $U_{24}Pp_{12}$ to goethite is much more dependent on the nanocluster concentration than hematite.

Using the observed reaction order terms, the sorption of $U_{24}Pp_{12}$ at pH 9 and 100 – 500 $m^2\ L^{-1}$ goethite and hematite can be described by equations 2 and 3, respectively,

$$\frac{d[U_{24}Pp_{12}]}{dt} = -k_{rxn}\,[U_{24}Pp_{12}]^{0.51\pm0.02}[\text{goethite}]^{0.61\pm0.03} \quad (2)$$

$$\frac{d[U_{24}Pp_{12}]}{dt} = -k_{rxn}\,[U_{24}Pp_{12}]^{0.12\pm0.01}[\text{hematite}]^{1.05\pm0.04} \quad (3)$$

where k_{rxn} for equation 2 is (5.3 ± 1.0) x 10^{-2} $(g\ L^{-1})^{0.51\pm0.02}(m^2\ L^{-1})^{-0.61\pm0.0.06}(day^{-1})$ and k_{rxn} for equation 3 is (1.8 ± 0.2) x 10^{-3} $(g\ L^{-1})^{0.88\pm0.01}(m^2\ L^{-1})^{-1.05\pm0.04}(day^{-1})$. For comparison, the rate law describing U_{60} sorption to goethite is provided in equation 4

$$\frac{d[U_{60}]}{dt} = -k_{rxn}\,[U_{60}]^{0.29\pm0.02}[\text{goethite}]^{1.2\pm0.1} \quad (4)$$

where $k_{rxn} = (6.7 \pm 2.0) \times 10^{-4}\ (g\ L^{-1})^{0.71\pm0.02}\ (m^2\ L^{-1})^{-1.2\pm0.1}(day^{-1})$.[10] A comparison of these rate laws shows that the sorption of $U_{24}Pp_{12}$ to goethite is faster than the sorption of $U_{24}Pp_{12}$ to hematite and the sorption of U_{60} to goethite. Since these nanoclusters appear to sorb as anions, the slower rate of sorption in the hematite system relative to the goethite system may be explained by the lower isoelectric point of hematite than goethite in this study (i.e., the IEP values are 9.13 ± 0.07 and 8.86 ± 0.06 for goethite and hematite, respectively). $U_{24}Pp_{12}$ may not interact with hematite as strongly as with goethite because the hematite surface is less positively charged than the goethite surface at pH 9. The functionality provided by the pyrophosphate linkages in the uranyl peroxide cage and the increased charge density of the nanocluster cage (relative to U_{60}) explains why the sorption of $U_{24}Pp_{12}$ is faster than the sorption of U_{60}.

Sorption at pH 8

In order to gain additional, corroborating information pertaining to the mechanisms governing $U_{24}Pp_{12}$ interactions with goethite and hematite, batch sorption experiments were also conducted at pH 8. The percentage of uranium removed from solutions containing 1.0 g L^{-1} $U_{24}Pp_{12}$ and 500 $m^2\ L^{-1}$ increased by 15% and 50% in systems containing goethite and hematite, respectively, when the pH dropped by one unit. The greater sorption increase in the system containing hematite compared to goethite is likely explained by the lower IEP of hematite. Since hematite has a lower IEP, changing the solution pH from 9 to 8 causes a greater increase in the amount of net positive surface potential compared to goethite. Since the hypothesized maximum sorption capacity (center-to-center spacing) of the nanoclusters on the goethite surface was nearly reached at pH 9, we would not expect a large change in the fraction sorbed when the pH is lowered to 8.

Thus, the mineral's net surface charge directly effects the sorption of $U_{24}Pp_{12}$. These results are similar to previous findings, which demonstrated an increase in the removal of U_{60} from solution with a decrease in pH in goethite and hematite suspensions.[12,13] At pH 8 the goethite and hematite surfaces will retain the greatest net positive charge, which attracts more of the negatively-charged $U_{24}Pp_{12}$ nanoclusters to the surface by electrostatic interactions and suggests that $U_{24}Pp_{12}$ behaves as an anionic species at the mineral-water interface.

Desorption and zeta potential measurements

Desorption experiments were conducted in order to examine the strength of $U_{24}Pp_{12}$ interactions with the mineral surfaces. Desorption experiments in systems containing 1 g L^{-1} $U_{24}Pp_{12}$ and 500 m^2 L^{-1} goethite and hematite revealed that sorption is not reversible at pH 7, 9 or 10. No desorption was observed when reacted minerals were suspended in Milli-Q water and only 2% and 5% desorption was achieved at pH 9 and 10 in systems containing goethite and hematite, respectively, within 5 days. These results were not expected given that $U_{24}Pp_{12}$ desorption occurs rapidly from artificial mesoporous silica[28] and approximately 20% of U_{60} is desorbed from goethite within three days at pH 10.[12] This suggests that $U_{24}Pp_{12}$ nanoclusters may form specific interactions with functional groups associated with hematite and goethite surfaces.

Electrophoretic mobility (EPM) measurements are useful for distinguishing inner- from outer-sphere complexes.[25] EPM measurements were performed for goethite and hematite samples that had been exposed to 1 g L^{-1} $U_{24}Pp_{12}$; the IEP shifts to 4.6 and 5.3 respectively (see Figure 2). A decrease in the EPM magnitude, and no change in the overall sign, would not necessarily distinguish between inner- or outer-sphere complexes. However, this shift to lower values is a strong, qualitative indicator for a specific interaction with surface sites because it implies that $U_{24}Pp_{12}$ sorption significantly altered the protonation behavior of the mineral surface.[25] The greater shift in the goethite system is likely due to the greater amount of $U_{24}Pp_{12}$ sorption. Charge reversal suggests that the sorbed nanocluster complexes are anionic in nature and bonded to goethite and hematite via non-electrostatic mechanisms such as covalent inner-sphere and/or hydrogen bonding. We monitored the solution phase for uranium, which was below detection limits due to the low rate of desorption described above. Thus, the measurements presented in Figure 2 recorded the EPM of the mineral-cluster particle complexes.

$U_{24}Pp_{12}$ associated with the mineral surface

Scanning electron microscopy with energy dispersive X-ray spectroscopy (SEM-EDS) was used to identify the presence and probe the distribution of U on the mineral surfaces.

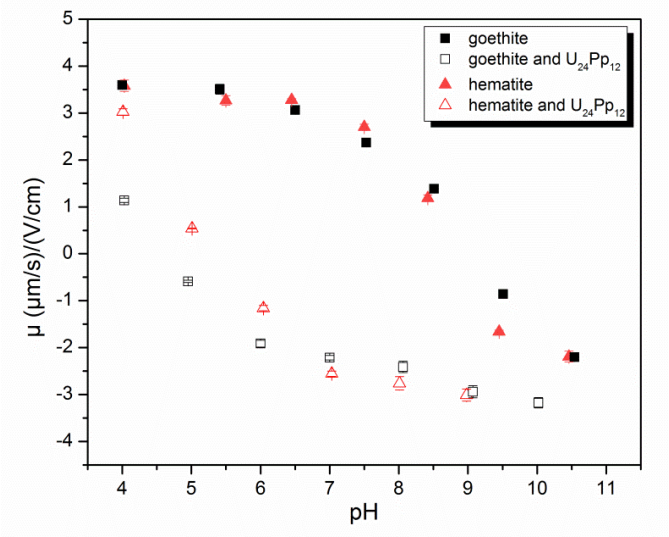

Figure 2. Electrophoretic mobility (μ) measurements as a function of pH for suspensions containing only goethite or hematite (closed symbols) and suspensions prepared from minerals that were exposed to 1 g L^{-1} $U_{24}Pp_{12}$ (open symbols). Standard deviations are reported from triplicate measurements.

SEM micrographs showed that the goethite crystals used in this study are acicular in shape (see Figure S9), which indicates that the 110 crystal face is predominant. There was sufficient removal of $U_{24}Pp_{12}$ in reactors containing goethite to measure U on the reacted goethite surface. In back-scatter-electron (BSE) mode, there was no evidence of precipitation of high-Z material on the surface of goethite (see Figure S10). To confirm elemental composition, EDS point spectra were obtained on multiple goethite particles to confirm a fairly even distribution of U (3.5 ± 1.5 wt. %). These results support the hypothesis of the sorption of discrete $U_{24}Pp_{12}$ nanoclusters to the surface, which is a homogeneous process by definition, and rules out the possibility of nanoclusters accumulating on the mineral surface as large aggregates or insoluble precipitates.

U 4*f*, Fe 2*p*, P 2*p*, Na 1*s*, O 1*s*, and Li 1*s* electrons were probed using X-ray photoelectron spectroscopy (XPS) to determine the elemental composition of each component on solids from systems containing 2 mg·mL^{-1} $U_{24}Pp_{12}$ and 500 $m^2 \cdot L^{-1}$ goethite or hematite. The Fe 2*p* envelope for goethite/hematite samples was fit without any contribution from Fe(II), confirming that the removal of nanoclusters from solution was not due to the reduction of the U(VI) to U(IV) by trace amounts of Fe(II).[29] On the reacted goethite surface, the U $4f_{5/2}$ peak occurred at 392.57 eV and U(VI) satellite peaks occurred at 395.93 eV and 402.55 eV (see Figure S12), which is in good agreement with published spectra.[30] P $2p_{3/2}$ and $2p_{1/2}$ peak positions occurred at 133.11 eV and 134.02 eV, respectively (see Figure S15), and the Na 1*s* peak occurred at 1071.51 eV (see Figure S18), which confirms the ICP-OES results discussed earlier. De-convolution of the main Li (1*s*) peak on the reacted goethite surface was difficult due to

the Fe 3*p* orbital overlap. XPS demonstrated that the uranium species deposited on the goethite surface is U(VI) with no contribution from U(IV) or U(V) and that phosphorous is also deposited on the goethite and hematite surfaces at a binding energy (~133 eV) that is indistinguishable from $U_{24}Pp_{12}$ crystals (see Figure S14) and common to standard pyrophosphate binding energies.[31] For hematite, the U $4f_{5/2}$ peak occurred at 392.81 eV and U(VI) satellites occurred at 396.46 eV and 402.76 eV (see Figure S13).

Attenuated total reflectance Fourier transform infrared spectroscopy (ATR-FTIR) was used to measure the phosphate-associated frequencies observed on air-dried goethite and hematite samples. Previous studies demonstrated that IR-active frequencies of adsorbed phosphate on damp and dried goethite samples are nearly indistinguishable.[32] The chemical environment of the phosphate-associated vibrational frequencies on dried goethite and hematite surfaces are different relative to crystals containing $U_{24}Pp_{12}$ (see Figure 3). Distinct shifts in the peak intensity and position suggest that P is in a unique chemical environment and that sorption may be occurring via the phosphorous-oxygen bonds truncating the nanocluster. The general similarity between the IR absorption peaks in the P-O stretching region of $U_{24}Pp_{12}$ sorbed to the mineral surfaces and the absorption peaks of $U_{24}Pp_{12}$ crystals suggests that $U_{24}Pp_{12}$ is present on the mineral surface. Only a fraction of terminating P-O bonds are participating in bonding interaction(s) with surface hydroxyl groups at a given time while the rest are positioned within the electric double layer.

The IR-active P-O stretching bands of crystals containing $U_{24}Pp_{12}$ occurred at 1164, 1097, 1033, and 988 cm^{-1} and are tentatively assigned as PO_3 (ν_{as}), P-O (ν), PO_3 (ν_s), and P-O-P (ν_{as}) terminal stretching modes, respectively.[18,33] In each case, the vibrational intensity of the terminating oxygen atoms (P-O, ν) of the pyrophosphate unit decreases relative to the PO_3 (ν_{as}) mode at a higher wavenumber. This decrease in relative intensity suggests that at least some fraction of the terminating oxygen atoms of the pyrophosphate unit are participating in bonding with the mineral surface. The significant decrease in the PO_3 (ν_s) and P-O-P (ν_{as}) stretching modes in the goethite system indicate a stronger interaction of $U_{24}Pp_{12}$ with the surface, in comparison to hematite, which restricts these vibrational modes. In both cases, the P-O-P (ν_{as}) stretching mode is blue-shifted, which indicates that this bond may be shortened slightly. The differences in the IR spectra also suggest that the $U_{24}Pp_{12}$ surface complexes are sensitive to the mineral crystallographic habit onto which they sorb due to the different surface binding groups that are available. The additional peak at 1175 cm^{-1} in the goethite system (Figure 3C) may be attributed to a P-O-H bending mode, which arises from interactions with surface hydroxyl groups.[23]

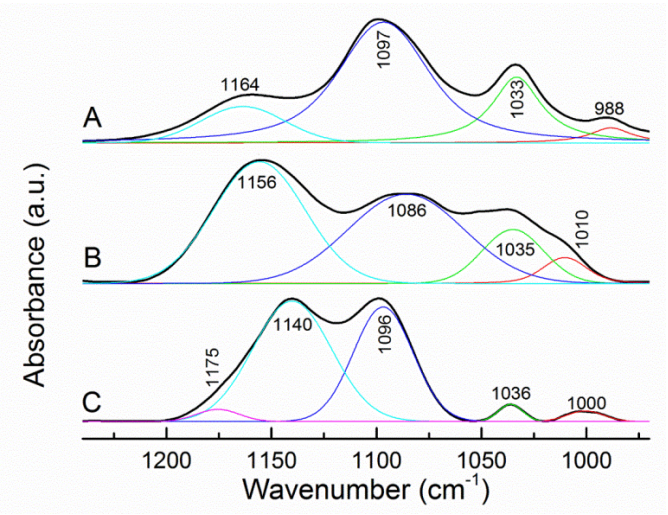

Figure 3. ATR-FTIR spectra of (A) $U_{24}Pp_{12}$ crystals, (B) hematite (500 m^2 L^{-1}) reacted with $U_{24}Pp_{12}$ (1 mg mL^{-1}) at pH 9, and (C) goethite (500 m^2 L^{-1}) reacted with $U_{24}Pp_{12}$ (1 mg mL^{-1}) at pH 9.

Raman spectroscopy was used to gain additional information about the uranium-species on the reacted hematite/goethite surface. Unlike in ATR-FTIR, the vibrational frequencies associated with hematite and goethite do not overlap with uranyl and peroxide stretching and vibrational modes in Raman. Raman spectra for $U_{24}Pp_{12}$ reacted with goethite after 2 days and $U_{24}Pp_{12}$ crystals dissolved in Milli-Q water are shown in Figures S21 and S22B, respectively. The spectral measurements confirmed the presence of uranyl species containing a peroxo group on the mineral surface. Raman signals at 809.5 and 853.2 cm^{-1} are assigned to the uranyl (U≡O) symmetric stretching mode and vibrations of the bridging peroxo groups (O-O), respectively, on the air-dried goethite surface. Both peaks are red-shifted compared to crystals containing $U_{24}Pp_{12}$. The uranyl symmetric stretching mode is shifted to a greater extent than the peroxide vibrational mode. This shift suggests that the uranyl bonds are elongated which may be attributed to the formation of stronger H-bonding interactions within the electric double layer of goethite than in solution or within a crystal lattice. This red-shifted uranyl symmetric stretch was also previously reported.[13]

Solutions containing 2 g L^{-1} $U_{24}Pp_{12}$ at pH 9 were allowed to air-dry and the resulting powder was compared to crystals containing $U_{24}Pp_{12}$ to confirm that these shifts are due to interactions with the mineral surface (see Figure S22). Given the low fraction of $U_{24}Pp_{12}$ removed at early time points and the lower amount removed in the presence of hematite, signals from the uranyl and peroxo groups in these systems were below the instrument detection limits.

$U_{24}Pp_{12}$ removal mechanism

The uranyl peroxide cage of $U_{24}Pp_{12}$ is truncated by uranyl oxygen atoms and the terminal oxygen atoms of the pyrophosphate unit (see Figure 1). ATR-FTIR, electrophoretic mobility measurements, and desorption experiments suggest that the nanocluster may be interacting with the mineral surfaces via specific, inner-sphere interactions. On the one hand, the collinear –yl oxygens are strongly bonded to U(VI), with ~1.6 valence units (*vu*) supplied to mostly satisfy the 2 *vu* requirement of O^{2-}.[34] A typical O-H bond provides ~0.8 *vu*, implying the –yl oxygen atoms are unlikely to be protonated. Although these –yl oxygens can act as H-bond acceptors and are often bound to highly-coordinated alkali cations in the crystalline phase, they are otherwise essentially chemically inert.[20] Consider the presence of the terminal oxygen atoms of the pyrophosphate units (Figure 1). The P-O bonds provide ~1.3 *vu* to each terminal O^{2-}, thus, it is possible for them to be protonated.[20,21] This bond valence deficiency can also be satisfied by accepting H-bond(s), and/or by bonding to alkali metal cations, implying that even if protonation were not to occur, the pyrophosphate groups could interact with the surface OH groups of goethite through stronger hydrogen bonding than is possible with –yl oxygens. The bond valence requirements of the other oxygen atoms in the pyrophosphate unit, either P-O-P or U-O-P, are largely met and they are unlikely to have any direct involvement in the sorption processes.

Crystallographic considerations of the surface hydroxyl configuration of goethite and hematite indicate that crystal plane terminating surface hydroxyl groups may be coordinated to one, two, or three underlying Fe atoms resulting in singly- ($\equiv FeOH^{-1/2}$), doubly- ($\equiv Fe_2OH$), and triply- ($\equiv Fe_3OH^{+1/2}$) coordinated groups.[35] These charges arise by assigning a +1/2 charge to each Fe-O bond, assuming six-fold coordination of the Fe atoms. Doubly-coordinated groups are generally considered to be inert because they do not carry a charge and are unreactive towards protonation, deprotonation, and ion binding in the pH range 2 – 12.[36]

Needle-shaped goethite crystals, such as those used in this study, are predominately comprised of the {110} crystal faces. The (110) face is dominated by triply-coordinated surface groups.[37] Per unit cell, there are three rows of triply-coordinated $Fe_3O(H)$ surface groups, one row of singly-coordinated FeOH(H) surface groups, and one row of doubly-coordinated Fe_2OH groups. The density of triply-coordinated hydroxyl groups on this crystal face is 9.1 groups nm^{-2},[35] however, one third of these sites are not protonated (i.e., $Fe_3O_{II}^{-1/2}$). Nevertheless, the remaining six groups per nm^2 (i.e., $=Fe_3O_IH^{+1/2}$) supply more than the number of reactive sites necessary to accommodate the amount of removed nanoclusters, given our conservative assumption of 2.3 sites nm^{-2}. These considerations suggest that the site-density calculations performed with our goethite sample are reasonable given the predominance of the {110} faces in our sample. The overall density of these groups on a particular crystal face varies from oxide to oxide and is also influenced by crystal morphology. The surface of hematite is comprised of numerous crystal planes and it becomes more difficult to determine the ideal bonding configuration in that system. For this reason, only goethite was considered in the following discussion.

Because triply-coordinated surface hydroxyl groups possess a +1/2 charge, they could mostly satisfy the bond valence deficiency of the terminating oxygen atoms of the pyrophosphate unit. In addition to these sites, singly-coordinated groups may be protonated a pHs below the IEP and act as a positively charged site (i.e., $FeOH_2^{+1/2}$).[37] Rows of contiguous singly-coordinated surface groups are considered to be involved in the specific adsorption of phosphate and other ions.[25,35] However, rows of singly-coordinated groups are separated by ~11 Å in the (110) plane direction. This would not allow for surface linkages by multiple terminal pyrophosphate ligands of an individual $U_{24}Pp_{12}$ nanocluster. Adsorption along the singly-coordinated rows is also unfavorable because the singly-coordinated groups are separated by ~3 Å in the *c* direction; the terminal oxygen atoms at the ends of each pyrophosphate unit are 4.9 Å apart, a distance that cannot overlay the singly-coordinated sites.

Crystallographic considerations were made by generating the ideal (110) crystal face of goethite using the BFDH morphology calculations in the Mercury software package,[38] using a previously determined structure.[39] Orienting the $U_{24}Pp_{12}$ cage to the crystal plane (Figure 4), reveals a physically optimal orientation between the macroion and the triply-coordinated reactive sites exposed on the (110) plane of goethite. This arrangement does not require chemical alteration of either the crystal solid or the macroion. Additionally, this orientation implies that interactions between the terminal oxygen atoms of the pyrophosphate unit ringing the hexagonal windows of the cage and the triply-coordinated hydroxyl groups are physically possible. This relatively complex configuration may be more reasonable than one where the nanocluster is bound through a lone pyrophosphate unit (i.e., two terminal oxygen atoms) interacting with singly-coordinated groups.

Conclusion

The purpose of this work was to compare the rate of $U_{24}Pp_{12}$ and U_{60} sorption to goethite and hematite and to describe how the inclusion of a proton-active functional group affects sorption behavior. Rate laws derived from batch sorption experiments indicate that the rate of uranyl peroxide nanocluster sorption may be dependent on the charge density and functionalized component of the uranyl peroxide cage. $U_{24}Pp_{12}$ is physically smaller and it also has a thinner electric double layer (which is consistent

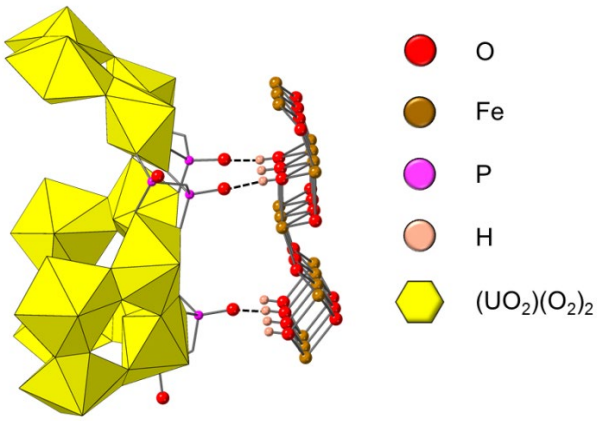

Figure 4. To-scale representation of the idealized $U_{24}Pp_{12}$ orientation on the (110) crystal face of goethite. The nanocluster is coordinated via the terminating oxygen atoms of the pyrophosphate unit to triply-coordinated functional OH groups. For clarity, part of the $U_{24}Pp_{12}$ cage has been cut away and only the top atomic layer of the (110) goethite plane is shown.

with its greater charge density) than U_{60}.[16,20] Thus, there are less steric constraints which might inhibit the sorption of $U_{24}Pp_{12}$ from both a physical and chemical perspective. $U_{24}Pp_{12}$ also contains pyrophosphate linkages with unsatisfied terminal oxygen atoms, which provide an avenue for specific interactions with a mineral surface.

An underlying hypothesis of our previous studies was that sorption interactions of non-functionalized uranyl peroxide nanoclusters would be similar due to the likeness of charge density between nanoclusters and the truncation of the uranyl peroxide cage by the unreactive -yl oxygen. Thus, U_{60} could be used as a surrogate to represent the sorption behavior of 'all' non-functionalized uranyl peroxide nanoclusters with roughly spherical cages. The results presented here provide the first evidence of a specific, inner-sphere complex at the (110) surface of goethite and suggest that nanocluster functionality and charge density play a substantial role in the sorption mechanisms. Therefore, uranyl peroxide nanoclusters containing other bridging ligands, such as phosphate, nitrate, oxalate, and phosphite, should be considered independently to gain a more comprehensive understanding of the mechanisms governing mineral-water interface chemistry and to provide a framework for building predictive models describing the mobility of uranyl peroxide nanoclusters in natural systems.

Conflicts of interest

There are no conflicts to declare.

Acknowledgements

This material is based on work supported by the Department of Energy, National Nuclear Security Administration as part of the Actinide Center of Excellence under Award Number DE-NA0003763. The authors thank Dr. Allen G. Oliver for helpful discussions regarding ATR-FTIR and Mercury analyses. The following centers and facilities at the University of Notre Dame provided access to instrumentation used in this research study: the Center for Environmental Science and Technology (BET, ICP-OES), the Mass Spectrometry and Proteomics Facility (ESI-MS), and the Center for Sustainable Energy's Materials Characterization Facility (powder X-ray diffraction, Raman, XPS).

References

1 *Blue Ribbon Commission on America's Nuclear Future Report to the Secretary of Energy*, Blue Ribbon Commission on America's Nuclear Future, 2012.
2 P. Bots, K. Morris, R. Hibberd, G. T. W. Law, J. F. W. Mosselmans, A. P. Brown, J. Doutch, A. J. Smith and S. Shaw, Formation of Stable Uranium(VI) Colloidal Nanoparticles in Conditions Relevant to Radioactive Waste Disposal, *Langmuir*, 2014, **30**, 14396–14405.
3 P. C. Burns and M. Nyman, Captivation with encapsulation: a dozen years of exploring uranyl peroxide capsules, *Dalton Trans.*, 2018, **47**, 5916–5927.
4 J. Qiu and P. C. Burns, Clusters of Actinides with Oxide, Peroxide, or Hydroxide Bridges, *Chem. Rev.*, 2013, **113**, 1097–1120.
5 K.-A. H. Kubatko, K. B. Helean, A. Navrotsky and P. C. Burns, Stability of Peroxide-Containing Uranyl Minerals, *Science*, 2003, **302**, 1191–1193.
6 C. R. Armstrong, M. Nyman, T. Shvareva, G. E. Sigmon, P. C. Burns and A. Navrotsky, Uranyl peroxide enhanced nuclear fuel corrosion in seawater, *Proc. Natl. Acad. Sci. U. S. A.*, 2012, **109**, 1874–1877.
7 P. C. Burns, R. C. Ewing and A. Navrotsky, Nuclear Fuel in a Reactor Accident, *Science*, 2012, **335**, 1184–1188.
8 M. E. McBriarty, J. A. Soltis, S. Kerisit, O. Qafoku, M. E. Bowden, E. J. Bylaska, J. J. De Yoreo and E. S. Ilton, Trace Uranium Partitioning in a Multiphase Nano-FeOOH System, *Environ. Sci. Technol.*, 2017, **51**, 4970–4977.
9 W. Um, R. J. Serne, C. F. Brown and K. A. Rod, Uranium(VI) sorption on iron oxides in Hanford Site sediment: Application of a surface complexation model, *Appl. Geochem.*, 2008, **23**, 2649–2657.
10 D. M. Sherman, C. L. Peacock and C. G. Hubbard, Surface complexation of U(VI) on goethite (alpha-FeOOH), *Geochim. Cosmochim. Acta*, 2008, **72**, 298–310.
11 A. Singh, K.-U. Ulrich and D. E. Giammar, Impact of phosphate on U(VI) immobilization in the presence of goethite, *Geochim. Cosmochim. Acta*, 2010, **74**, 6324–6343.
12 L. R. Sadergaski and A. E. Hixon, Kinetics of Uranyl Peroxide Nanocluster (U_{60}) Sorption to Goethite, *Environ. Sci. Technol.*, 2018, **52**, 9818–9826.
13 L. R. Sadergaski, W. Stoxen and A. E. Hixon, Uranyl Peroxide Nanocluster (U_{60}) Persistence and Sorption in the Presence of Hematite, *Environ. Sci. Technol.*, 2018, **52**, 3304–3311.
14 L. R. Sadergaski, M. Said and A. E. Hixon, Calcium-Facilitated Aggregation and Precipitation of the Uranyl

Peroxide Nanocluster U_{60} in the Presence of Na-Montmorillonite, *Environ. Sci. Technol.*, 2019, **53**, 4922–4930.

15 T. A. Olds, M. Dembowski, X. Wang, C. Hoffman, T. M. Alam, S. Hickam, K. L. Pellegrini, J. He and P. C. Burns, Single-Crystal Time-of-Flight Neutron Diffraction and Magic-Angle-Spinning NMR Spectroscopy Resolve the Structure and ^{1}H and ^{7}Li Dynamics of the Uranyl Peroxide Nanocluster U_{60}, *Inorg. Chem.*, 2017, **56**, 9676–9683.

16 K. M. Peruski, V. Bernales, M. Dembowski, H. L. Lobeck, K. L. Pellegrini, G. E. Sigmon, S. Hickam, C. M. Wallace, J. E. S. Szymanowski, E. Balboni, L. Gagliardi and P. C. Burns, Uranyl Peroxide Cage Cluster Solubility in Water and the Role of the Electrical Double Layer, *Inorg. Chem.*, 2017, **56**, 1333–1339.

17 M. Sharifironizi, J. E. S. Szymanowski, J. Qiu, S. Castillo, S. Hickam and P. C. Burns, Charge Density Influence on Enthalpy of Formation of Uranyl Peroxide Cage Cluster Salts, *Inorg. Chem.*, 2018, **57**, 11456–11462.

18 M. Dembowski, C. A. Colla, S. Hickam, A. F. Oliveri, J. E. S. Szymanowski, A. G. Oliver, W. H. Casey and P. C. Burns, Hierarchy of Pyrophosphate-Functionalized Uranyl Peroxide Nanocluster Synthesis, *Inorg. Chem.*, 2017, **56**, 5478–5487.

19 S. L. Flynn, J. E. S. Szymanowski, M. Dembowski, P. C. Burns and J. B. Fein, Experimental measurements of U24Py nanocluster behavior in aqueous solution, *Radiochimica Acta*, 2016, **104**, 853–864.

20 M. Dembowski, T. A. Olds, K. L. Pellegrini, C. Hoffmann, X. Wang, S. Hickam, J. He, A. G. Oliver and P. C. Burns, Solution ^{31}P NMR Study of the Acid-Catalyzed Formation of a Highly Charged $\{U_{24}Pp_{12}\}$ Nanocluster, $[(UO_2)_{24}(O_2)_{24}(P_2O_7)_{12}]^{48-}$, and Its Structural Characterization in the Solid State Using Single-Crystal Neutron Diffraction, *J. Am. Chem. Soc.*, 2016, **138**, 8547–8553.

21 R. L. Johnson, C. A. Ohlin, K. Pellegrini, P. C. Burns and W. H. Casey, Dynamics of a Nanometer-Sized Uranyl Cluster in Solution, *Angew. Chem., Int. Ed.*, 2013, **52**, 7464–7467.

22 B. T. McGrail, G. E. Sigmon, L. J. Jouffret, C. R. Andrews and P. C. Burns, Raman Spectroscopic and ESI-MS Characterization of Uranyl Peroxide Cage Clusters, *Inorg. Chem.*, 2014, **53**, 1562–1569.

23 U. Schwertmann and R. M. Cornell, *Iron Oxides in the Laboratory: Preparation and Characterization*, VCH Publishers, Inc., New York, NY, 1991.

24 A. S. Madden, M. F. Hochella Jr. and T. P. Luxton, Insights for size-dependent reactivity of hematite nanomineral surfaces through Cu2+ sorption, *Geochim. Cosmochim. Acta*, 2006, **70**, 4095–4104.

25 Z. Nie, N. Finck, F. Heberling, T. Pruessmann, C. Liu and J. Lützenkirchen, Adsorption of Selenium and Strontium on Goethite: EXAFS Study and Surface Complexation Modeling of the Ternary Systems, *Environ. Sci. Technol.*, 2017, **51**, 3751–3758.

26 J. A. Davis and D. B. Kent, in *Mineral-Water Interface Geochemistry*, eds. M. F. Hochella, Jr. and A. F. White, Mineralogical Society of America, Washington, DC, 1990, vol. 23, pp. 177–260.

27 M. Villalobos, M. A. Trotz and J. O. Leckie, Variability in goethite surface site density: evidence from proton and carbonate sorption, *J. Colloid Interface Sci.*, 2003, **268**, 273–287.

28 Y. Liu, A. Czarnecki, J. E. S. Szymanowski, G. E. Sigmon and P. C. Burns, Extraction behaviors of uranyl peroxo cage clusters by mesoporous silica SBA-15, *J Radioanal Nucl Chem*, 2016, **310**, 453–462.

29 T.-C. Lin, G. Seshadri and J. A. Kelber, A consistent method for quantitative XPS peak analysis of thin oxide films on clean polycrystalline iron surfaces, *Appl. Surf. Sci.*, 1997, **119**, 83–92.

30 M. Schindler, F. C. Hawthorne, M. S. Freund and P. C. Burns, XPS spectra of uranyl minerals and synthetic uranyl compounds. I: The U 4f spectrum, *Geochim. Cosmochim. Acta*, 2009, **73**, 2471–2487.

31 J. F. Moulder, W. F. Stickle, P. E. Sobol and K. D. Bomben, *Handbook of X-ray Photoelectron Spectroscopy: A Reference Book of Standard Spectra for Identification and Interpretation of XPS Data*, Perkin-Elmer Corporation, Eden Prairie, Minnesota, 1992.

32 J. D. Kubicki, K. W. Paul, L. Kabalan, Q. Zhu, M. K. Mrozik, M. Aryanpour, A.-M. Pierre-Louis and D. R. Strongin, ATR–FTIR and Density Functional Theory Study of the Structures, Energetics, and Vibrational Spectra of Phosphate Adsorbed onto Goethite, *Langmuir*, 2012, **28**, 14573–14587.

33 I. Kanesaka, K. Ozaki and I. Matsuura, Polarized Raman Spectra and Intensity Analysis of $Na_4P_2O_7$. $10H_2O$ and P-O stretches in $(VO)_2P_2O_7$, *Journal of Raman Spectroscopy*, 1995, **26**, 997–1002.

34 P. C. Burns, R. C. Ewing and F. C. Hawthorne, THE CRYSTAL CHEMISTRY OF HEXAVALENT URANIUM: POLYHEDRON GEOMETRIES, BOND-VALENCE PARAMETERS, AND POLYMERIZATION OF POLYHEDRA, *Can. Mineral.*, 1997, **35**, 1551–1570.

35 V. Barron and J. Torrent, Surface hydroxyl configuration of various crystal faces of hematite and goethite, *J. Colloid Interface Sci.*, 1996, **177**, 407–410.

36 T. Hiemstra and W. H. Van Riemsdijk, A Surface Structural Approach to Ion Adsorption: The Charge Distribution (CD) Model, *Journal of Colloid and Interface Science*, 1996, **179**, 488–508.

37 P. Venema, T. Hiemstra and W. H. van Riemsdijk, Multisite Adsorption of Cadmium on Goethite, *Journal of Colloid and Interface Science*, 1996, **183**, 515–527.

38 C. F. Macrae, P. R. Edgington, P. McCabe, E. Pidcock, G. P. Shields, R. Taylor, M. Towler and J. van de Streek, *Mercury*: visualization and analysis of crystal structures, *J Appl Cryst*, 2006, **39**, 453–457.

39 H. Yang, R. Lu, R. T. Downs and G. Costin, Goethite, α-FeO(OH), from single-crystal data, *Acta Cryst E*, 2006, **62**, i250–i252.

Evidence for non-electrostatic interactions between a pyrophosphate-functionalized uranyl peroxide nanocluster and iron (hydr)oxide minerals

Luke R. Sadergaski, Samuel N. Perry, Luke R. Tholen, and Amy E. Hixon*

Department of Civil and Environmental Engineering and Earth Sciences, University of Notre Dame, Notre Dame, Indiana 46556 USA
*Corresponding author: ahixon@nd.edu

Table of Contents Entry:

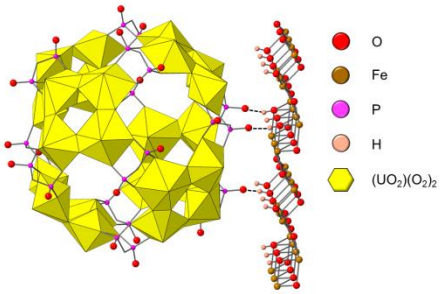

Electrophoretic mobility measurements and ATR-FTIR provide the first evidence of non-electrostatic interactions between a uranyl-based polyoxometalate and iron oxide surface.